Sensor requirements for in situ imaging of multiple damage by Lamb waves

E. Chan[1] L. R. Francis Rose[2] C. H. Wang[3]

(Received 19 December 2013; revised 7 June 2014)

Abstract

Lamb waves are guided waves that propagate in plate-like structures. These waves are well suited for wide-area inspection, such as aircraft wing skins, because of their relatively slow geometrical decay with propagation distance. Recently, a computationally efficient algorithm for in situ imaging was derived based on the multi-static data matrix. Here, previous work on imaging a single circular inhomogeneity is extended to the case of structural damage spread over two distinct sites. Detailed results are presented for the rank and bandwidth of the data matrix, showing the dependence on the overall size of the damage cluster. The implications of these results for the practically important problem of determining minimum sensor requirements for image reconstruction are discussed.

http://journal.austms.org.au/ojs/index.php/ANZIAMJ/article/view/7852
gives this article, © Austral. Mathematical Soc. 2014. Published July 19, 2014, as part of the Proceedings of the 11th Biennial Engineering Mathematics and Applications Conference. ISSN 1446-8735. (Print two pages per sheet of paper.) Copies of this article must not be made otherwise available on the internet; instead link directly to this URL for this article.

Contents

1 Introduction

The quantitative characterisation of structural damage is of significant importance to the continual assurance of structural integrity of aircraft structures, such as load-carrying thin-walled stiffened wing skins. With pertinent knowledge about damage location, geometry, size and severity, the structure's fatigue life and residual strength can be assessed with established predictive tools.

Structural health monitoring (SHM) employs a distributed network of on-board sensors, to interrogate the candidate structure autonomously and systematically with diagnostic Lamb wave signals. Lamb waves have gained significant interest as an efficient means for wide-area damage surveillance. The waves employed are tuned to propagate in appropriate modes to ensure optimum sensitivity to the anticipated damage mode and size.

An imaging technique based on digital beam formation predicted the location

of a single damage area by combining individual receiver-actuator pair images created from cross-correlation of the scattered Lamb wave signals and the interrogating pulse [1]. Time-shift algorithms and minimum variance techniques were also employed to process Lamb wave scattered field signals and find the location of a damage in a complex plate-like structure [2, 3]. Density maps created from time-of-flight of scattered Lamb wave signals were used to illustrate the probability of damage occurrence and hence its location in a composite structure [4].

More recently, in situ imaging methods, such as one based on diffraction tomography, were employed to image damage in a structure and hence quantify the damage characteristics [5, 6]. For such imaging methods, a computationally efficient algorithm based on the multi-static data matrix K, which gives the scattered field at a receiver location n due to a unit input at a source location j, was derived to image a single area of damage [7, 8, 9]. Accurate reconstruction in terms of location, geometry and size of the damage was achieved for both flat and stiffened aluminium plates [7, 8, 9].

Here, previous work is extended to the case where the structural damage is spread over two distinct sites. With the view of adapting the diffraction tomography approach [5, 6] to determine the minimum number of active sensors that are required for image reconstructions consistent with the theoretical image resolution, detailed results are presented for the damage modelled as two circular regions of unequal size and severity. In particular, the rank and bandwidth of the data matrix K is determined. The severity is modelled as a reduction in plate thickness, as is appropriate for metal corrosion induced thinning.

2 Sensor configuration and data matrix

Consider a network of N_s actuators (sources), distributed at discrete positions X_j for $j = 1, \ldots, N_s$ along a closed curve Γ_s, and N_r sensors (receivers)

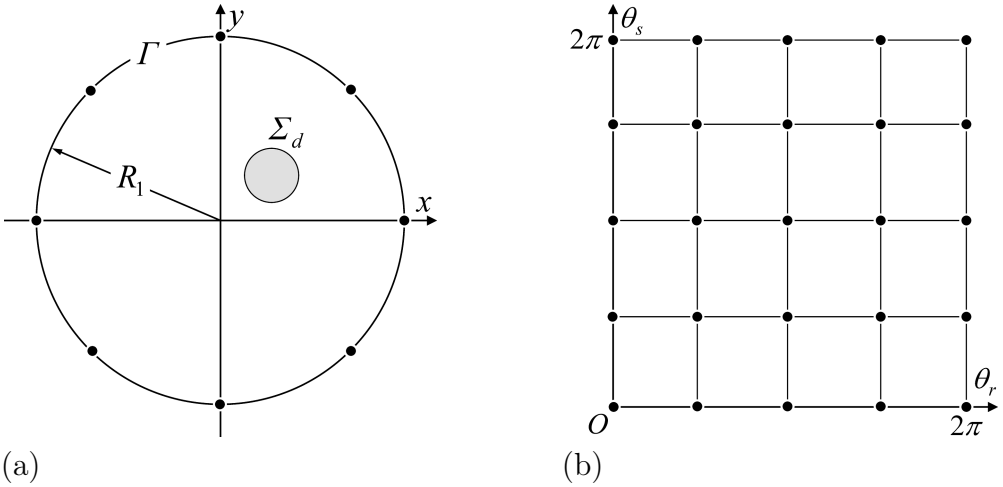

Figure 1: Concept of imaging. (a) Depiction of damage region and sensor array. (b) Illustration of discrete sampling of data matrix.

at locations $\mathbf{X}_n$ for $n = 1, \ldots, N_r$ along a possibly different curve Γ_r. For simplicity, active sensors serve the dual roles of actuators and sensors. The active sensors are thus distributed along a single closed curve $\Gamma = \Gamma_s = \Gamma_r$ as shown in Figure 1(a) and $N = N_s = N_r$.

Some damage is illustrated in Figure 1(a) by a shaded region marked by Σ_d. It is assumed that the structure suffers some form of in-plane damage. The total wave field at any location $\mathbf{x}$ in the structure due to a source at location $\mathbf{X}_j$ is

$$u(\mathbf{x}, \omega; \mathbf{X}_j) = u^I(\mathbf{x}, \omega; \mathbf{X}_j) + u^S(\mathbf{x}, \omega; \mathbf{X}_j)\,, \tag{1}$$

the superposition of incident wave field u^I and scattered wave field u^S due to the existence of damage. In the absence of damage, the scattered wave field is non-existent and $u^S = 0$. The total wave field $u(\mathbf{x}, \omega; \mathbf{X}_j)$ is a measured physical observable, such as the transverse deflection of a plate, that is, a Fourier transform at a particular angular frequency ω. It is assumed that the plate response is linear, even when damage is present.

The multi-static data matrix $\mathbf{K}$ contains all information about the damage and its elements are

$$\mathbf{K}_{nj}(\omega) = u^{S}(\mathbf{X}_n, \omega; \mathbf{X}_j)\,, \tag{2}$$

where the scattered wave field is recorded at sensor location $\mathbf{X}_n$ due to an incident wave originating from actuator location $\mathbf{X}_j$. The indices j and n in equations (1) and (2) are used to identify source and receiver locations, respectively. In Figure 1(b), the elements $\mathbf{K}_{nj}(\omega)$ are discrete samplings of the multi-static data function $\mathbf{K}(\theta_r, \theta_s)$ defined over the two dimensional domain, $0 \leqslant \theta_r\,,\ \theta_s < 2\pi$. If the active sensors are evenly distributed along Γ, then the resulting sampled data points are equispaced with respect to both source angle θ_s and receiver angle θ_r. For a chosen value of θ_r, $\mathbf{K}(\theta_r, \theta_s)$ is purely a function of source angle θ_s over an interval of 2π. If θ_s is defined beyond 2π, then the function would repeat itself in a periodic manner. Likewise, $\mathbf{K}(\theta_r, \theta_s)$ is a 2π periodic function of θ_r for a selected value of θ_s.

3 Case studies

Finite element (FE) modelling, with the software package Abaqus/Explicit [10], is used to simulate the Lamb waves and populate the data matrix $\mathbf{K}$. An aluminium flat plate with dimensions $400 \times 400 \times 1.6\,\text{mm}^3$, is considered. An evenly distributed network of 88 active sensors, located on a radius $R_1 = 75$ mm, in conjunction with a 200 kHz fundamental anti-symmetric wave mode, is used in sequence to interrogate the plate, before and after the presence of a region of inhomogeneity. The wave is initiated by an out-of-plane force of unit strength at a single FE node for source locations in the form of a five-cycle Hanning windowed sine wave. Additionally, the damage (inhomogeneity) is modelled as a region of thickness reduction, positioned symmetrical about the mid-plane of the plate. Uniform quadrilateral shell elements with mesh size of $0.5 \times 0.5\,\text{mm}^2$ were used in the simulations. The time-domain transverse displacements for the FE nodes acting as receivers

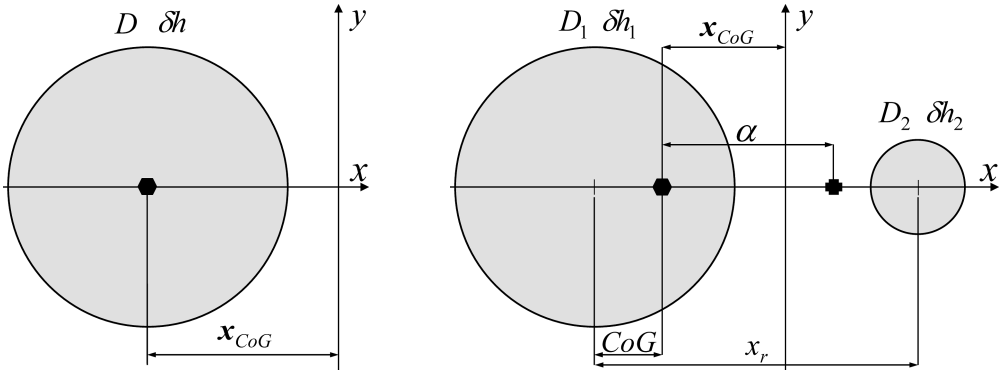

Figure 2: Damage configuration. (a) Single damage area. (b) Multiple damage areas.

were extracted at a sampling frequency of 2 MHz and time-gated to emulate the response from an infinitely large flat plate.

3.1 Rank and bandwidth for a single inhomogeneity

For a single inhomogeneity, the circular damage as depicted in Figure 2(a) has a diameter $D = 5\lambda$, where the wavelength $\lambda = 7.5\,\mathrm{mm}$, and a total thickness reduction $\delta h = 0.3\,\mathrm{mm}$. The centre of gravity (COG) of the damage is positioned at coordinates $(x_{COG}, 0)$.

The bandwidth of the data matrix K is evaluated with the discrete Fourier transform (DFT) of $K(\theta_r, \theta_s)$, for a fixed source at $\theta_s = \theta_j$ or fixed receiver at $\theta_r = \theta_n$:

$$\hat{K}(m, \theta_j) = \frac{1}{N} \sum_{n=1}^{N} K(\theta_n, \theta_j) \exp\left(\frac{-2i\pi mn}{N}\right), \quad \frac{-N}{2} \leqslant m < \frac{N}{2} - 1. \tag{3}$$

The entries to the DFT are simply the jth column or nth row of the data matrix K.

Figure 3(a) shows the DFT of the data matrix using the first row, that is Sensor #1, $\theta_r = 0$, for a single inhomogeneity positioned at $x_{COG} = -12.5\,\text{mm}$. The bandwidth B which is non-dimensional, is 26.4 and is defined as half the width at which the DFT has fallen to 0.1 of its maximum value. The nonzero DFT values outside the vertical dash lines in Figure 3(a) are due to FE modelling errors. Theoretically, these values should be zero. The DFT using the 23rd row of the data matrix, that is Sensor #23, $\theta_r = \pi/2$, is illustrated in Figure 3(b) and $B = 20.8$. The B values for Sensors #1 and #23 are the lower and upper extremes of the data matrix bandwidth. Further, the data matrix is amenable to a singular value decomposition (SVD) for which the numerical rank is defined as the number of singular values above a chosen threshold. As revealed in Figure 3(c), the calculated numerical rank is $R = 35$.

The bandwidth of the data matrix for a single scatterer is reduced to a minimum, such as that for COG of the inhomogeneity positioned at the centre of the sensor array, through *factorisation*. The *factorised* data matrix is

$$S_{nj} = \frac{K_{nj}}{\sigma G(\mathbf{X}_n, \mathbf{x}_0) G(\mathbf{x}_0, \mathbf{X}_j)}\,, \tag{4}$$

where σ is the strength of the scatterer and G represents the prevailing Green's function at the damage COG in the absence of any damage. The resulting DFT using the first and 23rd rows of the *factorised* data matrix is shown in Figure 3(d) and the bandwidth for both rows is reduced to about 18.

3.2 Rank and bandwidth for multiple inhomogeneities

Figure 2(b) shows two distinct circular damages of diameter $D_1 = 3\lambda$ and $D_2 = \lambda$, separated by a relative distance $x_r = 3\lambda$ and both located along the x-axis with COG of the damage cluster $(x_{COG}, 0)$. For the larger damage D_1, the reduction in thickness is $\delta h_1 = 0.3\,\text{mm}$. Whereas for D_2, $\delta h_2 = 0.2\,\text{mm}$. When compared to the previous example of a single damage area, the two

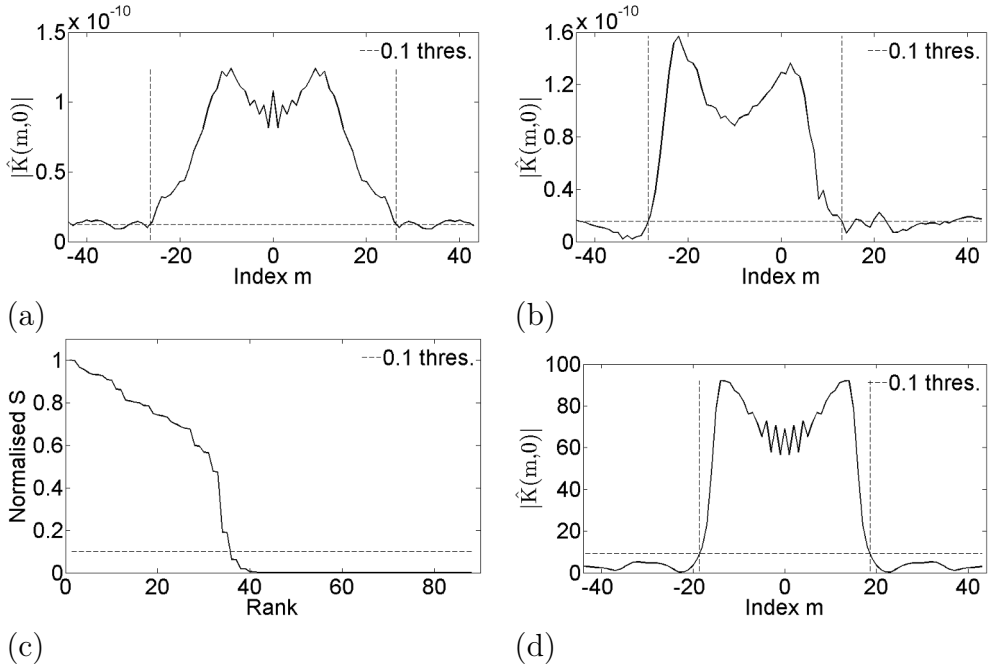

Figure 3: Rank and bandwidth for an off-centre single damage. (a) DFT first row $B = 26.4$. (b) DFT 23rd row $B = 20.8$. (c) SVD showing rank $R = 35$. (d) *Factorised* DFT first row $B = 18.1$.

damage areas in the current configuration reside within the diameter $D = 5\lambda$, that is D circumscribes D_1 and D_2.

The bandwidth for the data matrix are again calculated with equation (3) using the first and 23rd rows. The COG of the damage cluster is positioned at the centre of the sensor array. As revealed in Figure 4(a), the lower bandwidth is 10.9, and in Figure 4(b) the bandwidth is 15.8. The numerical rank is 25.

When the damage cluster is located away from the centre of the sensor array, the bandwidth increases but the rank remains unchanged. For damage located at $x_{COG} = -18.5\,\text{mm}$, the bandwidth calculated with the first row shown in Figure 5(a) and with the 23rd row, in Figure 5(b), is 19 and 17.3, respectively.

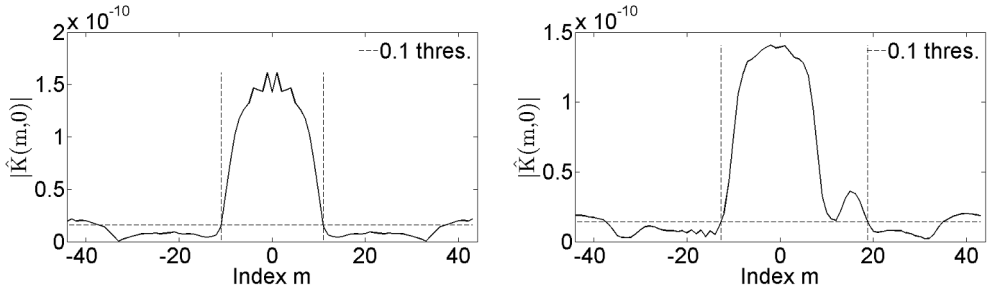

(a) (b)

Figure 4: Rank and bandwidth for multiple damage. (a) COG first row $B = 10.9$. (b) COG 23rd row $B = 15.8$.

The bandwidths, as revealed in Figures 5(c) and 5(d) are reduced to 10.9 using the first row and 16.7 for the 23rd row, when the data matrix is *factorised* by the Green's function for a pristine plate at the location of the damage cluster's COG.

4 Implications of results

Figure 6(a) shows the variation in bandwidth due to changes in position of a single damage area relative to the centre of the active sensor array. In this figure, the bandwidth of the original data matrix K increases as the location of the damage x_{COG} is moved further from the origin. Both bandwidth values, calculated with either the first or 23rd row, follow the same trend. However, the bandwidth of row one gradually becomes greater than that of row 23. Figure 6(a) also reveals that the bandwidth reduces to a minimum of approximately 17.5 when the data matrix is *factorised* by the appropriate Green's functions, that is, when the bandwidth is equivalent to that of damage located at the centre of the sensor array. It is apparent that both rows one and 23 illustrate the reduction in bandwidth for all values of x_{COG}.

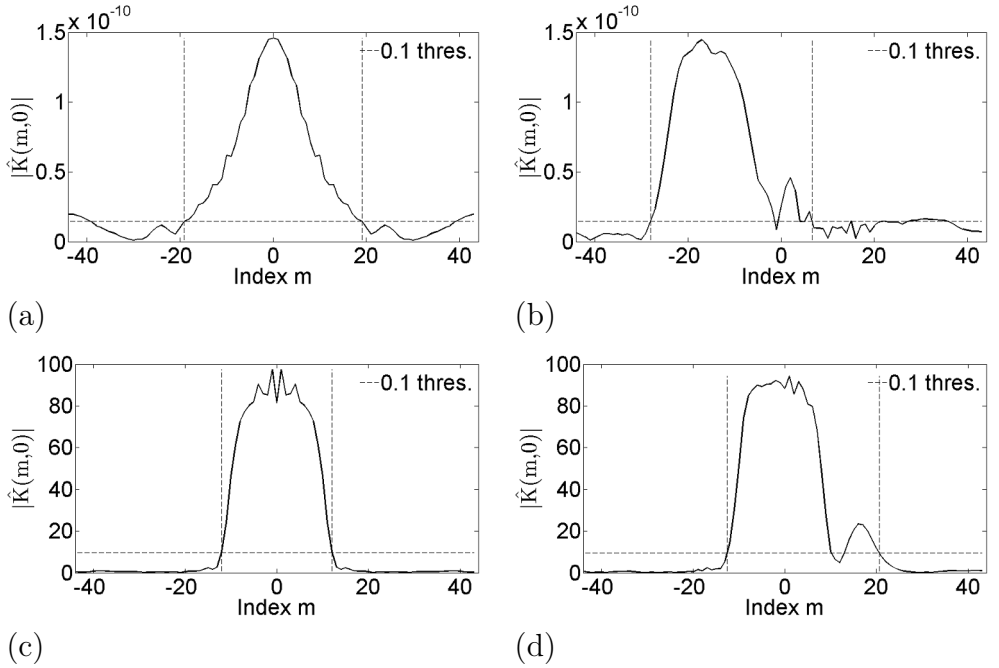

Figure 5: Rank and bandwidth for an off-centre multiple damage cluster. (a) DFT first row $B = 19$. (b) DFT 23rd row $B = 17.3$. (c) *Factorised* DFT first row $B = 10.9$. (d) *Factorised* DFT 23rd row $B = 16.7$.

From Figure 6(a), and supported by Wang and Rose [8], the minimum number of spatial viewing angles, and therefore number of sensors required for reconstruction of a single damage area, corresponds to the rank approximately equal to double the *bandwidth* $2B \approx R$. In view of this, approximately 36 sensors are needed for damage size D, regardless of its position relative to the origin.

In Figure 6(b), the bandwidth for a damage cluster with two circular damage areas, calculated using row one of the original data matrix, increases as the cluster is positioned further away from the sensor array origin. Here, the bandwidth increases linearly from 11 to 19 for x_{COG} values of 1.5 to −18.5 mm.

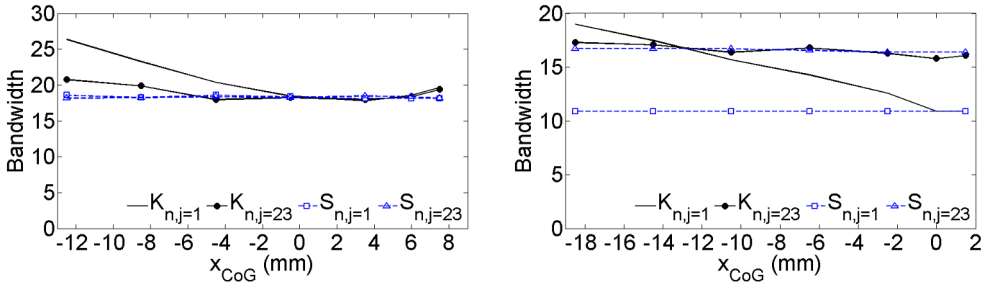

Figure 6: Variation of bandwidth for original and factorised data matrices. (a) Single damage. (b) Multiple damage.

However, the bandwidths calculated with row 23 of the original data matrix for the same x_{CoG} are almost constant and are approximately 16.5 and 17.5, respectively. *Factorising* the data matrix and recalculating the bandwidth results in reduced bandwidth for row one but not row 23. In Figure 6(b), for row one of the *factorised* data matrix, the bandwidth reduces to a minimum of about 11, regardless of the values of x_{CoG}. The bandwidth calculated using row 23 of the *factorised* data matrix remains generally unchanged and is similar to that calculated from the original data matrix. Similar to the case of a single damage area, about 36 sensors are required for imaging a cluster of two damage areas with sizes D_1 and D_2 and separated by relative distance x_r.

Unlike the configuration with a single damage area in which the bandwidth (and sensor requirement) are determined with any row or column from a *factorised* data matrix, the bandwidth for the case of multiple damage is dictated by the row (or column) that returns the greatest bandwidth. Figure 6(b) shows that the bandwidth for multiple damage areas is prescribed by row 23.

Despite both damage sizes D_1 and D_2 being smaller than D (for the case with a single damage area), the selected minimum bandwidth for the cases with single and multiple damage areas are approximately the same. This suggests that the bandwidth, corresponding to the number of sensors to use in

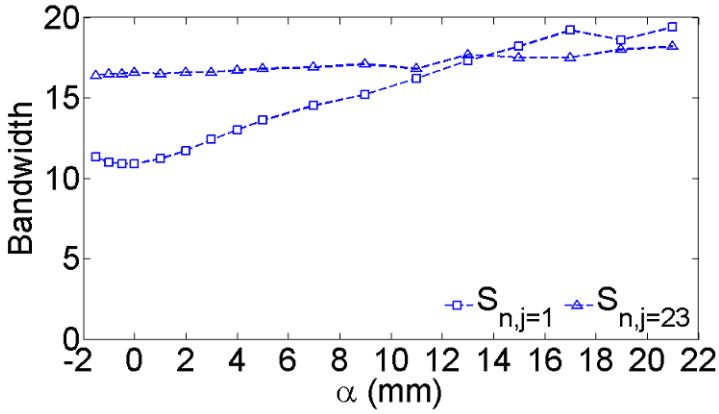

Figure 7: Variation in bandwidth for multiple damage *factorised* by a range of locations relative to the damage cluster χ_{COG}.

practice, is not only dictated by the size of the individual damage diameters, but the diameter of the entire damage cluster at the widest point, that is, the overall size of the damage cluster is the same as the single damage area.

From Figure 7, the minimum bandwidth is achieved when the data matrix is *factorised* by the prevailing Green's function at the exact location of the χ_{COG} of the damage cluster. In Figure 7, α, as illustrated in Figure 2(b), is the distance between the damage χ_{COG} and the location (and therefore Green's function) selected for *factorisation* along the χ-axis. In this example, the damage cluster and hence the χ_{COG} is positioned at the centre of the sensor array. The bandwidth evaluated with row one is at a minimum only when $\alpha = 0$. The bandwidth increases linearly on either side of the damage χ_{COG}.

In the context of SHM and damage imaging (characterisation), the least number of sensors that are capable of reconstructing the damage should be used to produce hi-fidelity images and to minimise system mass (and complexity), for a specific range of damage sizes as stipulated by airworthiness regulations. The current work shows that the spread of multiple damage (at least for the case of two circular inhomogeneities) as well as the damage cluster's overall

location relative to its $\mathbf{x}_{\text{COG}}$, are also variables that prescribe the number of sensors to be employed.

5 Summary

This article presents detailed results relating to the bandwidth and rank of the multi-static data matrix for the case where damage is spread over two distinct locations. The minimum number of sensors that is required in practice for adequate imaging performance is dictated by the bandwidth, which is reduced by a factorisation procedure, if the centre of gravity of the damage is known. The results calculated with data from FE simulations for a flat aluminium plate reveal that each individual damage size, the overall size of the damage cluster at the widest point, and the position selected for *factorisation* are variables contributing towards the minimum number of sensors required for imaging.

Acknowledgements This study was supported in part by an Australian Research Council Discovery Grant DP 120103430.

References

[1] C. T. Ng and M. Veidt. A Lamb-wave-based technique for damage detection in composite laminates. *Smart Mater. Struct.*, 18(7):074006, 2009. doi:10.1088/0964-1726/18/7/074006 C284

[2] J. E. Michaels and T. E. Michaels. Guided wave signal processing and image fusion for in situ damage localization in plates. *Wave Motion*, 44(6):482–192, 2007. doi:10.1016/j.wavemoti.2007.02.008 C284

[3] J. S. Hall and J. E. Michaels. Multi-path guided wave imaging for in situ monitoring of complex structures. *AIP Conf. Proc.* 1511:707-713, 2013. doi:10.1063/1.4789115 C284

[4] Z. Q. Su, L. Cheng, X. M. Wang and L. Yu. Diagnostic imaging for structural damage. *Adv. Mater. Res.*, 47–50:1157–1160, 2008. doi:10.4028/www.scientific.net/AMR.47-50.1157 C284

[5] L. R. F. Rose and C. H. Wang. Mindlin plate theory for damage detection: Source solutions. *J. Acoust. Soc. Am.*, 116(1):154–171, 2004. doi:10.1121/1.1739482 C284

[6] L. R. F. Rose and C. H. Wang. Mindlin plate theory for damage detection: Imaging of flexural inhomogeneities. *J. Acoust. Soc. Am.*, 127(2):754–763, 2010. doi:10.1121/1.3277217 C284

[7] C. H. Wang and L. R. F. Rose. Imaging damage using Mixed Passive and Active Sensors. *4th Asia-Pacific Workshop on Structural Health Monitoring, 2012*, Melbourne, Australia. C284

[8] C. H. Wang and L. R. F. Rose. Minimum Sensor Density for Quantitative Damage Imaging. *9th International Workshop on Structural Health Monitoring, 2013, Standford, USA*. C284, C291

[9] E. Chan, C. H. Wang and L. R. F. Rose. Characterisation of Part-through Damage in a Stiffened Panel by a Time-reversal Based Imaging Method. *9th International Workshop on Structural Health Monitoring, 2013, Standford, USA*. C284

[10] Abaqus/Explicit 6.10 *Dassault Systemes* http://www.3ds.com/products-services/simulia/portfolio/abaqus/abaqus-portfolio/abaqusexplicit/ C286

Author addresses

1. **E. Chan**, School of Aerospace, Mechanical and Manufacturing Engineering, RMIT University, GPO Box 2476, Melbourne, Victoria 3001 Australia.
mailto:s3230884@student.rmit.edu.au

2. **L. R. Francis Rose**, School of Aerospace, Mechanical and Manufacturing Engineering, RMIT University, GPO Box 2476, Melbourne, Victoria 3001 Australia.

3. **C. H. Wang**, School of Aerospace, Mechanical and Manufacturing Engineering, RMIT University, GPO Box 2476, Melbourne, Victoria 3001 Australia.